Submitted to the Special Session of Adaptive Aeroelastic Wing Shaping Control

Wing Shaping and Gust Load Controls of Flexible Aircraft: An LPV Approach

Jared R. Hammerton* and Weihua Su†

University of Alabama, Tuscaloosa, Alabama, 35487-0280

Gouming Zhu‡

Michigan State University, East Lansing, Michigan, 48824

Sean Shan-Min Swei§

NASA Ames Research Center, Moffett Field, California, 94035

Extended Abstract

Overview

In the proposed paper, the optimum wing shape of a highly flexible aircraft under varying flight conditions will be controlled by a linear parameter-varying approach. The optimum shape determined under multiple objectives, including flight performance, ride quality, and control effort, will be determined as well. This work is an extension of work done previously by the authors, and updates the existing optimization and utilizes the results to generate a robust flight controller.

I. Introduction

The improvement of aircraft operation efficiency needs to be considered over the whole flight plan, instead of a single point in the flight envelope, since the flight condition varies in a flight mission. Therefore, it is natural to employ morphing wing designs so that the aircraft can be made adaptive to different flight conditions and missions. At the advent of recent development in advanced composites as well as sensor and actuator technologies,

*Graduate Research Assistant, Department of Aerospace Engineering and Mechanics, jrhammerton@ua.edu, Member AIAA.

†Assistant Professor, Department of Aerospace Engineering and Mechanics, suw@eng.ua.edu, Senior Member AIAA.

‡Professor, Department of Mechanical Engineering, zhug@egr.msu.edu.

§Research Scientist, Intelligent Systems Division, sean.s.swei@nasa.gov, Member AIAA.

in-flight adaptive wing/aircraft morphing is now becoming a tangible goal. Traditionally, the discrete control surfaces were used to re-distribute the aerodynamic loads along the wing span during the flight, so as to tailor the aircraft performance. However, the deflection of discrete control surfaces may increase the aerodynamic drag. An effective alternative is to introduce conformal wing/airfoil shape changes for the aerodynamic load control. In addition, the flexibility associated to the morphing wing structures may be pro-actively utilized to improve the aircraft performance. The active aeroelastic tailoring techniques would allow aircraft designers to take advantage of the wing flexibility to create the desired wing load distribution according to the mission requirement, so as to improve overall aircraft operating efficiency and performance, without using the traditional discrete control surfaces. The utilization of these concepts is predicated upon the optimum shape being known and a control system which is able to produce this wing shape.

The question of determining the optimum wing shape has been studied in depth. Recently, Chen et al.[1] studied the effects of various trim conditions on the aerodynamic shape optimization of the common research model wing-body-tail configuration. Using a free form distribution for the wing geometry coupled with a RANS solver for the aerodynamics their work studied the impact of a trim constraint on the optimization process. Through a series of optimizations utilizing the trim conditions at varying points in the design process, they concluded that considering the trim during optimization yields the best performance. In a similar study, Lyu and Martins[2] performed an aerodynamic optimization of the trailing edge of wing. Their optimization showed that drag reductions could be seen with shape optimization of either the entire wing or just the trailing edge. Taking the optimization a step further requires the development of realistic system capable of producing the optimum shape that is found for a given flight condition. This concept is shown in,[3] as the major aspects of the design of the Variable Camber Continuous Trailing Edge Flap (VCCTEF) are highlighted. Along with this detailed design an optimization is performed to determine the deflection angles required throughout the trailing edge to improve the flight performance.

More detailed concepts of wing morphing technologies have been developed as improvements in the materials being used on aircraft and the methods in which they are assembled has improved. In Nguyen et al.[4] the principles of aerodynamic shape optimization and morphing wing structures was explored. The optimization process led into the development of the VCCTEF, which was a novel concept for improving aircraft performance by drag reduction. A further study of the VCCTEF wing model was done by Nguyen and Ting,[5] where they performed a flutter analysis of the mission adaptive wing. The methodology included a vortex-lattice aerodynamic model coupled with a finite element structural dynamic model. Urnes et al.[6] provided an updated review of the development, design, and testing of the VCCTEF project. Under the support of the U.S. Air Force Research Laboratory, FlexSys, Inc. developed the Mission Adaptive Compliant Wing (MAC-Wing) to test and evaluate its performance. The adaptive trailing edge flap technology was combined with a natural laminar flow airfoil and tested on the Scaled Composites White Knight aircraft. The testing suggested fuel saving, weight reduction, and improved control authority.[7,8] In an effort to move from an adaptable trailing edge into a completely adaptable wing structure, the Cellular Composite Active Twist Wing was designed and tested in[9] showing promising results. An airplane model was built, which incorporated two of the active twist wing and was compared to a similar rigid model with traditional control surfaces in wind-tunnel tests. The active twist wing showed similar capabilities for symmetric and asymmetric movements as well as

added benefits in stall mitigation. An overview of the process used to design the composite lattice-based cellular structures for active wing shaping was presented in Jenett et al.[10] This paper gave a detailed approach to design a low density, highly complaint structure. The detailed modeling and construction of these structures was also presented.

As optimization processes and morphing technology have improved, there is a need for a complete system, in which a controller will actuate the wing members to the desired optimum shape throughout the entire flight envelope and perform the required maneuver and vibration control during the flight. Most current optimization schemes utilize a CFD aerodynamic model coupled with discrete structural points as design variables. These methods produce promising results, but when considered over an entire flight plan could be a very time consuming process. Additionally, these methods generally consider the planform shape of the wing rather than the wing bending and torsions associated with highly flexible, large aspect ratio wing members. Recent developments of morphing technologies such as the Cellular Composite Active Twist Wing take advantage of the flexible nature of high aspect ratio wings. Therefore, it is natural to develop an optimization scheme that mainly considers the bending and torsion of the high aspect ratio wings. This concept was utilized in Su et al.,[11] which utilized a modal based optimization approach in determining the best feasible wing shape (wing bending and torsion deformations) of a highly flexible aircraft at any given flight scenario. In this paper, this process will be used going forward to develop a wing shape control algorithm with defined distributed control loads. The optimization process will generate the specific wing shape needed to guarantee the optimum performance and ride quality over the entire flight envelope of an aircraft. Since there are no conventional discrete control surfaces for trimming and control the flexible aircraft, the design space for searching the optimum wing geometry is enlarged. The optimum wing shape obtained from the modal-based optimization also naturally leads to a distributed controller. At the same time, this also leaves a lot of degrees of freedom in the controller design. In addition, the controller should satisfy the performance and stability requirements over variable flight conditions, which is typically required for mission-adaptive vehicles. In doing so, the controller will be designed based on a linear parameter-varying (LPV) method, derived from the nonlinear aeroelastic equations representing the highly flexible aircraft.

II. Theoretical Formulation

A coupled aeroelastic and flight dynamic formulation for highly flexible aircraft has been developed by Su and Cesnik.[12–14] A brief introduction of the formulation is presented here, followed by the modal-based optimization approach for searching the most efficient wing geometries with the optimum distributed control scheme along the wing span under different flight conditions.

A. Equations of motion

As shown in figure 1a, a global(inertia) frame G is defined. A body frame $B(t)$ is then built in the global frame to describe the vehicle position and orientation. By taking advantage of their geometry, highly flexible wings are modeled as slender beams that may exhibit large deformations in operation. Within the body frame, a local beam frame w is built at each node along the reference line (figure 1b), which is used to define the nodal position

and orientation of the flexible members. In Su and Cesnik,[15] a nonlinear beam element has been introduced to model the geometrically-nonlinear deformation of slender beams. In this formulation, strain degrees (curvatures) of the beam reference line are considered as the independent variables to describe the beam deformation. Assume the curvatures are constant within one element, the elemental strain vector is denoted as

$$\varepsilon_e^T = \left\{ \begin{array}{cccc} \varepsilon_x & \kappa_x & \kappa_y & \kappa_z \end{array} \right\} \tag{1}$$

where ε_x is the extensional strain, κ_x, κ_y, and κ_z are the twist curvature of the beam reference line, out-of-plane bending curvature, and in-plane bending curvature, respectively. The total strain vector of the complete aircraft ε is obtained by assembling the global strain vector. Transverse shear strains are not explicitly included in this equation. However, shear strain effects are included in the constitutive relation.[16] Complex geometrically nonlinear deformations can be represented by such a constant-strain distribution over each element.

By following the Principle of Virtual Work extended to dynamic systems, the coupled aeroelastic and flight dynamic behavior of highly flexible aircraft in free flight can be described by the following equations:

$$\begin{aligned} \mathbf{M}_{FF}(\varepsilon)\ddot{\varepsilon} + \mathbf{M}_{FB}(\varepsilon)\dot{\beta} + \mathbf{C}_{FF}(\dot{\varepsilon},\varepsilon,\beta)\dot{\varepsilon} + \mathbf{C}_{FB}(\dot{\varepsilon},\varepsilon,\beta)\beta + \mathbf{K}_{FF}\varepsilon \\ = \mathbf{R}_F(\ddot{\varepsilon},\dot{\varepsilon},\varepsilon,\dot{\beta},\beta,\lambda,\zeta,\mathbf{T},\mathbf{u}) \\ \mathbf{M}_{BF}(\varepsilon)\ddot{\varepsilon} + \mathbf{M}_{BB}(\varepsilon)\dot{\beta} + \mathbf{C}_{BF}(\dot{\varepsilon},\varepsilon,\beta)\dot{\varepsilon} + \mathbf{C}_{BB}(\dot{\varepsilon},\varepsilon,\beta)\beta \\ = \mathbf{R}_B(\ddot{\varepsilon},\dot{\varepsilon},\varepsilon,\dot{\beta},\beta,\lambda,\zeta,\mathbf{T},\mathbf{u}) \\ \dot{\zeta} = -\frac{1}{2}\Omega_\zeta(\beta)\zeta \\ \dot{\mathbf{P}}_B = \left[\begin{array}{cc} \mathbf{C}^{GB}(\zeta) & \mathbf{0} \end{array} \right]\beta \\ \dot{\lambda} = \mathbf{F}_1 \left\{ \begin{array}{c} \ddot{\varepsilon} \\ \dot{\beta} \end{array} \right\} + \mathbf{F}_2 \left\{ \begin{array}{c} \dot{\varepsilon} \\ \beta \end{array} \right\} + \mathbf{F}_3\lambda \end{aligned} \tag{2}$$

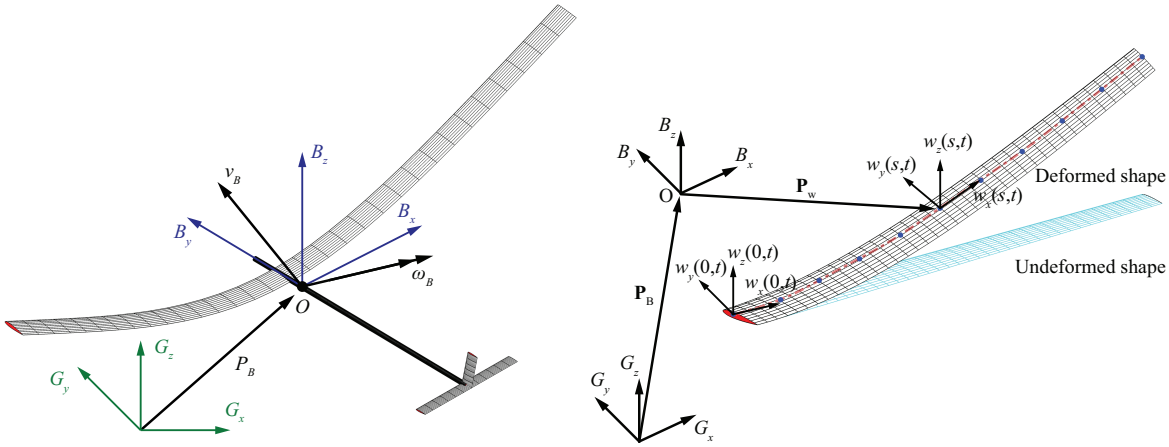

(a) Global and body frames defining the rigid-body motion of aircraft

(b) Flexible lifting-surface frames within body frame

Figure 1: Basic beam reference frames

where the components of the generalized inertia $\mathbf{M}$, damping $\mathbf{C}$, and stiffness $\mathbf{K}$ matrices are found in.[12,13] in general, gravity, aerodynamic loads, thrust, and control forces are considered in the generalized load vector of aircraft, which is given as

$$\begin{aligned}\left\{ \begin{array}{c} \mathbf{R}_F \\ \mathbf{R}_B \end{array} \right\} = \left\{ \begin{array}{c} \mathbf{K}_{FF}\varepsilon^0 \\ 0 \end{array} \right\} + \left[\begin{array}{c} \mathbf{J}_{p\varepsilon}^T \\ \mathbf{J}_{pb}^T \end{array} \right] \mathbf{B}^F\mathbf{F}^a + \left[\begin{array}{c} \mathbf{J}_{\theta\varepsilon}^T \\ \mathbf{J}_{\theta b}^T \end{array} \right] \mathbf{B}^M\mathbf{M}^a \\ + \left[\begin{array}{c} \mathbf{J}_{h\varepsilon}^T \\ \mathbf{J}_{hb}^T \end{array} \right] \mathbf{N}^g\mathbf{g} + \left[\begin{array}{c} \mathbf{J}_{p\varepsilon}^T \\ \mathbf{J}_{pb}^T \end{array} \right] \mathbf{T} + \left[\begin{array}{c} \bar{\mathbf{B}}_F \\ \bar{\mathbf{B}}_B \end{array} \right] \mathbf{u}\end{aligned} \tag{3}$$

which involves the effects from initial strains ε^0, aerodynamic loads $\mathbf{F}^a$ and $\mathbf{M}^a$, gravitational fields $\mathbf{g}$, thrust force $\mathbf{T}$, and additional control input $\mathbf{u}$. $\mathbf{B}^F$, $\mathbf{B}^M$, and $\mathbf{N}^g$ are the influence matrices for aerodynamic lift, moment, and gravity force, respectively, which come from the numerical integration of virtual work done by the external loads along the wing span (see Su and Cesnik[12]). Influence matrices of the control input ($\bar{\mathbf{B}}_F$ and $\bar{\mathbf{B}}_B$) are dependent on the specific control mechanism and are yet to be determined in this paper. Finally, all the Jacobian matrices $\mathbf{J}$ in Eq. (3) can be obtained from the nonlinear strain-position kinematic relationship discussed in,[15,17] which link the dependent variables (nodal positions and orientations) to the independent variables (element strain and rigid-body motion). It should be noted that both elastic member deformations and rigid-body motions are included when deriving the internal and external virtual work in Su and Cesnik.[12] Therefore, the elastic (ε) and rigid-body (β) degrees of freedom are naturally coupled. This coupling is also highlighted in Eq. (2), where the elastic deformations and the rigid-body motions are solved from the same set of equations.

In Eq. (3), aerodynamics loads are calculated by using the 2-D finite-state inflow theory.[18] At a given station along the wing, the aerodynamics lift, moment, and drag are given as

$$\begin{aligned} l_{mc} &= \pi\rho_\infty b_c^2\left(-\ddot{z} + \dot{y}\dot{\alpha} - d\ddot{\alpha}\right) + 2\pi\rho_\infty b_c\dot{y}^2\left[-\frac{\dot{z}}{\dot{y}} + \left(\frac{1}{2}b_c - d\right)\frac{\dot{\alpha}}{\dot{y}} - \frac{\lambda_0}{\dot{y}}\right] \\ m_{mc} &= \pi\rho_\infty b_c^2\left(-\frac{1}{8}b_c^2\ddot{\alpha} - \dot{y}\dot{z} - d\dot{y}\dot{\alpha} - \dot{y}\lambda_0\right) \\ d_{mc} &= -2\pi\rho_\infty b_c\left(\dot{z}^2 + d^2\dot{\alpha}^2 + \lambda_0^2 + 2d\dot{z}\dot{\alpha} + 2\dot{z}\lambda_0 + 2d\dot{\alpha}\lambda_0\right)\end{aligned} \tag{4}$$

where the inflow states λ are governed by the inflow equation in Eq. (2). The different velocity components referred by Eq. (4) can be seen in Fig. 2.

B. Definition of general distributed control load

In the current study, a distributed control scheme is developed by assuming every element along the main wing can be actuated. Figure 3 shows a generic wing element with applied point force (u_1) and force couplings (ru_2, ru_3 and ru_4) on both ends in order to actuate it. The combined loads may independently actuate the extensive, torsional, out-of-plane bending, and in-plane bending deformations of the element. These elemental loads are written as

$$\begin{aligned}\left(\mathbf{F}_u^{pt}\right)_e &= \left\{ \begin{array}{cccccccccc} -u_1 & 0 & 0 & 0 & 0 & 0 & u_1 & 0 & 0 \end{array} \right\}^T \\ \left(\mathbf{M}_u^{pt}\right)_e &= \left\{ \begin{array}{cccccccccc} -ru_2 & -ru_3 & -ru_4 & 0 & 0 & 0 & ru_2 & ru_3 & ru_4 \end{array} \right\}^T\end{aligned} \tag{5}$$

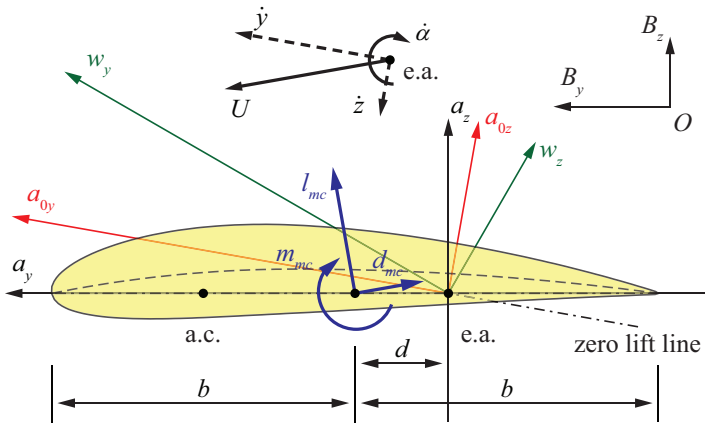

Figure 2: Airfoil coordinate systems and velocity components

where the coefficient r represents the arms of force couplings u_1, u_2, and u_3. Without losing generality, r is defined as one in the following studies. Note that there are three nodes defined on each beam element.[15] As no loads are applied at the mid-node of the element for the actuation, the fourth to sixth entries of the load vectors are all zeros. Eq. (5) is further written into the matrix form of

$$\begin{aligned}
\left(\mathbf{F}_u^{pt}\right)_e &= \begin{bmatrix} -1 & 0 & 0 & 0 & 0 & 0 & 1 & 0 & 0 \\ 0 & 0 & 0 & 0 & 0 & 0 & 0 & 0 & 0 \\ 0 & 0 & 0 & 0 & 0 & 0 & 0 & 0 & 0 \\ 0 & 0 & 0 & 0 & 0 & 0 & 0 & 0 & 0 \end{bmatrix}^T \begin{Bmatrix} u_1 \\ u_2 \\ u_3 \\ u_4 \end{Bmatrix} = \left(\mathbf{B}_u^f\right)_e \mathbf{u}_e \\
\left(\mathbf{M}_u^{pt}\right)_e &= \begin{bmatrix} 0 & 0 & 0 & 0 & 0 & 0 & 0 & 0 & 0 \\ -1 & 0 & 0 & 0 & 0 & 0 & 1 & 0 & 0 \\ 0 & -1 & 0 & 0 & 0 & 0 & 0 & 1 & 0 \\ 0 & 0 & -1 & 0 & 0 & 0 & 0 & 0 & 1 \end{bmatrix}^T \begin{Bmatrix} u_1 \\ u_2 \\ u_3 \\ u_4 \end{Bmatrix} = \left(\mathbf{B}_u^m\right)_e \mathbf{u}_e
\end{aligned} \tag{6}$$

Accordingly, the complete control loads are obtained by properly sizing and assembling the elemental matrices in Eq. (6), which are

$$\begin{aligned}
\mathbf{F}_u^{pt} &= \mathbf{B}_u^f \mathbf{u} \\
\mathbf{M}_u^{pt} &= \mathbf{B}_u^m \mathbf{u}
\end{aligned} \tag{7}$$

where $\mathbf{F}_u^{pt}$ and $\mathbf{M}_u^{pt}$, as point loads, can be eventually transformed to the generalized control load by using the Jacobians:

$$\begin{aligned}
\begin{Bmatrix} \mathbf{R}_F^u \\ \mathbf{R}_B^u \end{Bmatrix} &= \begin{bmatrix} \mathbf{J}_{p\varepsilon}^T \\ \mathbf{J}_{pb}^T \end{bmatrix} \mathbf{F}_u^{pt} + \begin{bmatrix} \mathbf{J}_{\theta\varepsilon}^T \\ \mathbf{J}_{\theta b}^T \end{bmatrix} \mathbf{M}_u^{pt} \\
&= \left(\begin{bmatrix} \mathbf{J}_{p\varepsilon}^T \\ \mathbf{J}_{pb}^T \end{bmatrix} \mathbf{B}_u^f + \begin{bmatrix} \mathbf{J}_{\theta\varepsilon}^T \\ \mathbf{J}_{\theta b}^T \end{bmatrix} \mathbf{B}_u^m \right) \mathbf{u} = \begin{bmatrix} \bar{\mathbf{B}}_F \\ \bar{\mathbf{B}}_B \end{bmatrix} \mathbf{u}
\end{aligned} \tag{8}$$

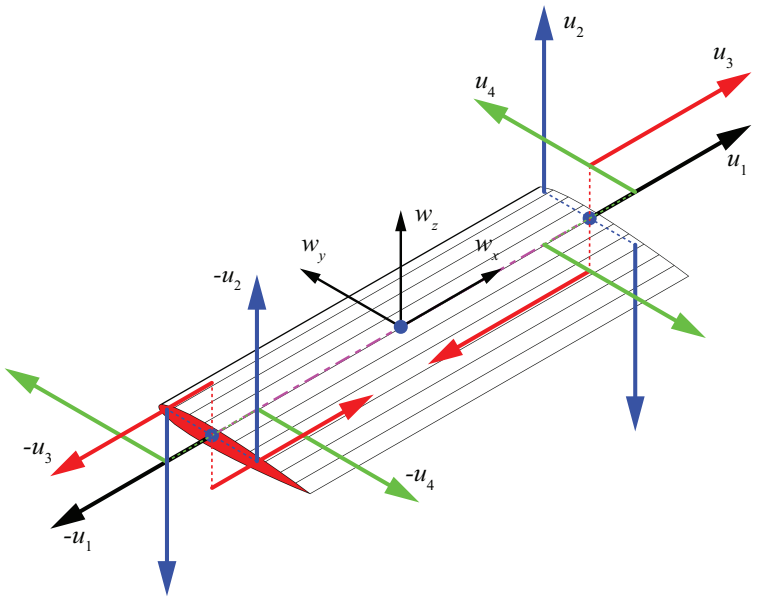

Figure 3: Point control forces on a beam element (Black: extension force; Blue: torsion coupling; Red: out-of-plane bending coupling; and Green: in-plane bending coupling).

C. Determination of optimum wing geometry

Under a given flight condition (U_∞ and ρ), the optimum wing geometry and other control inputs should be determined to satisfy the trim of aircraft. In general, the trim variables are:

$$q_{trim} = \left\{ \begin{array}{cccc} \alpha_B & \varphi_B & \mathbf{T} & \mathbf{u} \end{array} \right\}^T \tag{9}$$

where α_B is the body pitching angle, φ_B is the bank angle, and $\mathbf{u}$ is the control input as defined in Sec. B. With the rigid-body rotation angles, one can prescribe the quaternions and rigid-body velocity:

$$\begin{aligned} \zeta &= \zeta(\alpha_B, \varphi_B) \\ \beta &= \beta(U_\infty, \zeta) \end{aligned} \tag{10}$$

Therefore, the original aeroelastic and flight dynamic equations (Eq. 2) are reduced to steady-state equilibrium equations, after removing the transient terms and unsteady aerodynamic contributions, which are

$$\begin{aligned} \mathbf{K}_{FF}\varepsilon - \mathbf{R}_F(\alpha_B, \varphi_B, \mathbf{T}, \mathbf{u}, \varepsilon) &= \mathbf{0} \\ \mathbf{R}_B(\alpha_B, \varphi_B, \mathbf{T}, \mathbf{u}, \varepsilon) &= \mathbf{0} \end{aligned} \tag{11}$$

where the loads are explicitly determined by the trim variables, as well as the wing shape. It is clear that the second entry of Eq. (11) is essentially the trim condition that an aircraft in steady flight should satisfy, while the first is the elastic equilibrium only for flexible aircraft.

In the study of Su et al.,[11] a modal-based approach was developed to search for the optimum wing geometry without using the traditional control surfaces. This approach is still utilized here, where the wing geometry is represented by linear mode shapes, such that

$$\bar{\varepsilon}(s,t) = \sum_{i=1}^{N} \Phi_i(s)\eta_i(t) \tag{12}$$

where Φ are the linear mode shapes of the flexible aircraft and η are the corresponding magnitudes of the modes. This approach allows one to use a finite number of modes to search for the optimum wing shape, targeting for the minimum drag as the optimum flight performance, while maintaining the trim and elastic equilibrium of the aircraft.

$$\begin{aligned} \mathbf{r}_F &= \mathbf{K}_{FF}\bar{\varepsilon} - \mathbf{R}_F(\alpha_B, \varphi_B, \mathbf{T}, \mathbf{u}, \eta_1, \eta_2, \cdots, \eta_N) \\ \mathbf{r}_B &= \mathbf{R}_B(\alpha_B, \varphi_B, \mathbf{T}, \mathbf{u}, \eta_1, \eta_2, \cdots, \eta_N) \end{aligned} \tag{13}$$

From Eq. (13) and Eq. (8) the control force $\mathbf{u}$ can be calculated during each step of the optimization process as

$$\mathbf{u} = \bar{\mathbf{B}}_F^{-1}\left(\mathbf{K}_{FF}\bar{\varepsilon} - \mathbf{J}_{p\varepsilon}^T\mathbf{B}^F\mathbf{F}^a - \mathbf{J}_{\theta\varepsilon}^T\mathbf{B}^M\mathbf{M}^a - \mathbf{J}_{h\varepsilon}^T\mathbf{N}^g\mathbf{g} - \mathbf{J}_{p\varepsilon}^T\mathbf{T}\right) \tag{14}$$

With the elastic equilibrium now satisfied, the optimization problem is defined as

$$\begin{aligned} &\min_q D = D(q) \\ &s.t. \quad \mathbf{r}_B = 0 \\ &q = \left\{ \begin{array}{cccccccc} \alpha_B & \varphi_B & \mathbf{T} & \eta_1 & \eta_2 & \cdots & \eta_N \end{array} \right\}^T \end{aligned} \tag{15}$$

D. Multi-objective optimization

It may be desired to determine a shape which accomplishes a goal other than minimizing drag. Highly-flexible aircraft with slender wings are often susceptible to the effects of a gust. To account for this, another objective function is required so as to minimize the wing bending moment due to gust disturbances. This function will then be combined with the minimum drag objective to formulate a multi-objective optimization problem. This allows for a study to be performed to understand the various shapes required to find the trade-off between the minimum drag and the minimum gust effects.

A discrete gust model is used to calculate the moment a gust could generate on root of the wing. The gust should have a width 25 times longer than the chord of the wing, which for this particular study would result in a gust that is 25 meters long. The gust velocity can be expressed as here

$$w_{gust} = \frac{w_0}{2}\left(1 - cos\left(\frac{2\pi x}{25c}\right)\right) \tag{16}$$

To further simplify the problem a method similar to[19] will be used. This reduces the gust so that the entire streamwise length of the airfoil section experiences the same value of the gust velocity at a given time. This gives an effective angle of attack as expressed here

$$\alpha_g = \frac{1}{2}\frac{w_0}{U_\infty}\left(1 - cos\left(\frac{2\pi x}{25c}\right)\right) \tag{17}$$

The maximum angle of attack will occur as

$$(\alpha_g)_{max} = \frac{w_0}{U_\infty} \tag{18}$$

from which the resulting aerodynamic loads can be calculated.

The alleviation of the gust load can be approximated by minimizing the induced bending moment M_y at the root of the wing. Using this along with the aerodynamic drag calculation used in the single objective function optimization the new objective function can be defined as

$$f_{obj} = \xi D + (1 - \xi) M_y \tag{19}$$

Additionally it is desired to implement a third objective function which accounts for the control effort required to obtain a specific wing geometry. The control force required is already calculated and described in Eq. (14). The total control effort can then be approximated as

$$\mathbf{U} = \mathbf{u}^T \mathbf{u} \tag{20}$$

E. Optimum reduced control scheme – location of actuations

As can be seen, Eq. (8) defines the control loads on all elements of the flexible aircraft. Therefore, all these elements should be actuated to achieve and maintain the optimum wing geometry for the best performance. Obviously, this control scheme requires a tremendous number of actuations along the vehicle, which ends up being impractical. Instead, one can select a reduced set of elements from the aircraft (and more effectively on the main wing) to control the wing shape. From Eq. (12), the wing shape has been represented by the mode shapes. It is natural to examine the "controllability" of these modes. For shaping and rigid-body motion control purpose, Eq. (2) is reduced to structural dynamic equations coupled with the rigid-body motion, with all aerodynamic loads, thrust force, and gravity loads removed. The body frame propagation equations are not required as the rigid-body motions are represented by β, which leads to

$$\begin{aligned} \mathbf{M}_{FF}\ddot{\varepsilon} + \mathbf{M}_{FB}\dot{\beta} + \mathbf{C}_{FF}\dot{\varepsilon} + \mathbf{C}_{FB}\beta + \mathbf{K}_{FF}\varepsilon &= \bar{\mathbf{B}}_F \mathbf{u} \\ \mathbf{M}_{BF}\ddot{\varepsilon} + \mathbf{M}_{BB}\dot{\beta} + \mathbf{C}_{BF}\dot{\varepsilon} + \mathbf{C}_{BB}\beta &= \bar{\mathbf{B}}_B \mathbf{u} \end{aligned} \tag{21}$$

$$\begin{bmatrix} \mathbf{M}_{FF} & \mathbf{M}_{FB} \\ \mathbf{M}_{BF} & \mathbf{M}_{BB} \end{bmatrix} \begin{Bmatrix} \ddot{\varepsilon} \\ \dot{\beta} \end{Bmatrix} + \begin{bmatrix} \mathbf{K}_{FF} & \mathbf{0} \\ \mathbf{0} & \mathbf{0} \end{bmatrix} \begin{Bmatrix} \varepsilon \\ \mathbf{b} \end{Bmatrix} = \bar{\mathbf{B}}\mathbf{u} \tag{22}$$

One may write Eq. (21) into the state-space form:

$$\begin{Bmatrix} \dot{\varepsilon} \\ \ddot{\varepsilon} \\ \dot{\beta} \end{Bmatrix} = \mathbf{A}_s \begin{Bmatrix} \varepsilon \\ \dot{\varepsilon} \\ \beta \end{Bmatrix} + \mathbf{B}_s \mathbf{u} \tag{23}$$

where

$$\begin{aligned} \mathbf{A}_s &= \begin{bmatrix} \mathbf{I} & \mathbf{0} & \mathbf{0} \\ \mathbf{0} & \mathbf{M}_{FF} & \mathbf{M}_{FB} \\ \mathbf{0} & \mathbf{M}_{BF} & \mathbf{M}_{BB} \end{bmatrix}^{-1} \begin{bmatrix} \mathbf{0} & \mathbf{I} & \mathbf{0} \\ -\mathbf{K}_{FF} & -\mathbf{C}_{FF} & -\mathbf{C}_{FB} \\ \mathbf{0} & -\mathbf{C}_{BF} & -\mathbf{C}_{BB} \end{bmatrix} \\ \mathbf{B}_s &= \begin{bmatrix} \mathbf{I} & \mathbf{0} & \mathbf{0} \\ \mathbf{0} & \mathbf{M}_{FF} & \mathbf{M}_{FB} \\ \mathbf{0} & \mathbf{M}_{BF} & \mathbf{M}_{BB} \end{bmatrix}^{-1} \begin{bmatrix} \mathbf{0} \\ \bar{\mathbf{B}}_F \\ \bar{\mathbf{B}}_B \end{bmatrix} \end{aligned} \tag{24}$$

The controllability of the modes of $\mathbf{A}_s$ in terms of the control input determined by $\mathbf{B}_s$ can be measured. This measure exploits the angles between the normalized left eigenvectors $\mathbf{R}_i$ of the system matrix $\mathbf{A}_s$ and the control input influence matrix $\mathbf{B}_s$.[20] The measure of controllability of the ith mode by the jth actuator is

$$\cos\theta_{ij} = \frac{|\mathbf{R}_i \cdot \mathbf{b}_j|}{\|\mathbf{R}_i\| \, \|\mathbf{b}_j\|} \tag{25}$$

where $\mathbf{b}_j$ is the jth column vector of matrix $\mathbf{B}_s$. If the fraction is one (i.e., $\theta_{ij} = 0$), it achieves the maximum controllability of mode $\mathbf{R}_i$ by actuator j.

In search for the optimum shape under a flight condition, one can first explore the optimum shape assuming the fully-distributed control using Eq. (15), which results in an optimum wing shape represented by the mode shapes Φ_i and the corresponding magnitudes η_i. Based on the magnitudes, one may decide what modes are more significant than the others. Next, the controllability of these significant modes are evaluated. A specific controller (nodal control force entry) is retained in the $\bar{\mathbf{B}}_F$ and $\bar{\mathbf{B}}_B$, only if its control impacts to the significant modes are above a user-defined threshold value. Such a selection results in a reduced control scheme $\bar{\mathbf{B}}_{Fr}$ or $\bar{\mathbf{B}}_{Br}$. The distributed control force can be calculated at each step of the optimization as

$$\mathbf{u}_r = \bar{\mathbf{B}}_{Fr}^{-1}\left(\mathbf{K}_{FF}\bar{\varepsilon} - \mathbf{J}_{p\varepsilon}^T\mathbf{B}^F\mathbf{F}^a - \mathbf{J}_{\theta\varepsilon}^T\mathbf{B}^M\mathbf{M}^a - \mathbf{J}_{h\varepsilon}^T\mathbf{N}^g\mathbf{g} - \mathbf{J}_{p\varepsilon}^T\mathbf{T}\right) \tag{26}$$

The optimization of the wing shape with the objective of the minimum drag Eq. (15) can be performed again with the reduced control input scheme where one can solve for the magnitudes (η_i) of the modes contributing to the optimum wing geometry under the reduced control input $\mathbf{u}_r$. It is also necessary to verify if the significant modes from the second optimization are consistent with the initial search with the full-distributed control scheme. Additional iterative processes can be performed, if the significant modes become inconsistent with the reduced control input applied.

Finally, it is important to note that the optimum reduced control scheme may vary under different flight conditions, as the participating modes to determine the optimum wing shape are different.

F. State-space equations

Linearized aeroelastic and flight dynamic equations of motion about a nonlinear equilibrium state χ_0 are obtained as

$$\begin{aligned}
\bar{\mathbf{M}}_{FF}\ddot{\bar{\varepsilon}} + \bar{\mathbf{M}}_{FB}\dot{\beta} + \bar{\mathbf{C}}_{FF}\dot{\bar{\varepsilon}} + \bar{\mathbf{C}}_{FB}\beta + \bar{\mathbf{K}}_{FF}\varepsilon - \mathbf{R}^a_{F/\lambda} - \mathbf{R}^g_{F/\zeta} &= \bar{\mathbf{B}}_{Fr}\mathbf{u}_r \\
\bar{\mathbf{M}}_{BF}\ddot{\bar{\varepsilon}} + \bar{\mathbf{M}}_{BB}\dot{\beta} + \bar{\mathbf{C}}_{BF}\dot{\bar{\varepsilon}} + \bar{\mathbf{C}}_{BB}\beta - \mathbf{R}^a_{B/\lambda} - \mathbf{R}^g_{B/\zeta} &= \bar{\mathbf{B}}_{Br}\mathbf{u}_r \\
\dot{\zeta} + \frac{1}{2}\Omega_\zeta\zeta + \frac{1}{2}\left(\Omega_{\zeta/\beta}\beta\right)\zeta_0 &= \mathbf{0} \\
\dot{\mathbf{P}}_B - \begin{bmatrix} \mathbf{C}^{GB} & \mathbf{0} \end{bmatrix}\beta - \begin{bmatrix} \mathbf{C}^{GB}_{/\zeta}\zeta & \mathbf{0} \end{bmatrix}\beta_0 &= \mathbf{0} \\
\dot{\lambda} - \mathbf{F}_1\begin{Bmatrix} \ddot{\bar{\varepsilon}} \\ \dot{\beta} \end{Bmatrix} - \mathbf{F}_2\begin{Bmatrix} \dot{\bar{\varepsilon}} \\ \beta \end{Bmatrix} - \mathbf{F}_3\lambda &= \mathbf{0}
\end{aligned} \tag{27}$$

which is put into the state-space form

$$\begin{aligned}\dot{\mathbf{x}} &= \mathbf{Q}_1^{-1}\mathbf{Q}_2\mathbf{x} + \mathbf{Q}_1^{-1}\mathbf{Q}_3\mathbf{u}_r \\ &= \mathbf{A}\mathbf{x} + \mathbf{B}\mathbf{u}_r\end{aligned} \tag{28}$$

where the state variable is

$$\mathbf{x}^T = \left\{ \begin{array}{cccccc} \varepsilon^T & \dot{\varepsilon}^T & \beta^T & \zeta^T & \mathbf{P}_B^T & \lambda^T \end{array} \right\} \tag{29}$$

and the matrices for calculating the system matrices are

$$\begin{aligned}
\mathbf{Q}_1 &= \begin{bmatrix} \mathbf{I} & \mathbf{0} & \mathbf{0} & \mathbf{0} & \mathbf{0} & \mathbf{0} \\ \mathbf{0} & \bar{\mathbf{M}}_{FF} & \bar{\mathbf{M}}_{FB} & \mathbf{0} & \mathbf{0} & \mathbf{0} \\ \mathbf{0} & \bar{\mathbf{M}}_{BF} & \bar{\mathbf{M}}_{BB} & \mathbf{0} & \mathbf{0} & \mathbf{0} \\ \mathbf{0} & \mathbf{0} & \mathbf{0} & \mathbf{I} & \mathbf{0} & \mathbf{0} \\ \mathbf{0} & \mathbf{0} & \mathbf{0} & \mathbf{0} & \mathbf{I} & \mathbf{0} \\ \mathbf{0} & -\mathbf{F}_{1F} & -\mathbf{F}_{1B} & \mathbf{0} & \mathbf{0} & \mathbf{I} \end{bmatrix} \\
\mathbf{Q}_2 &= \begin{bmatrix} \mathbf{0} & \mathbf{I} & \mathbf{0} & \mathbf{0} & \mathbf{0} & \mathbf{0} \\ -\bar{\mathbf{K}}_{FF} & \bar{\mathbf{C}}_{FF} & \bar{\mathbf{C}}_{FB} & \mathbf{R}^g_{F/\zeta} & \mathbf{0} & \mathbf{R}^a_{F/\lambda} \\ \mathbf{0} & \bar{\mathbf{C}}_{BF} & \bar{\mathbf{C}}_{BB} & \mathbf{R}^g_{B/\zeta} & \mathbf{0} & \mathbf{R}^a_{B/\lambda} \\ \mathbf{0} & \mathbf{0} & -\frac{1}{2}\left(\Omega_{\zeta/\beta}\right)\zeta_0 & -\frac{1}{2}\Omega_\zeta & \mathbf{0} & \mathbf{0} \\ \mathbf{0} & \mathbf{0} & \begin{bmatrix} \mathbf{C}^{GB} & \mathbf{0} \end{bmatrix} & \begin{bmatrix} \mathbf{C}^{GB}_{/\zeta} & \mathbf{0} \end{bmatrix}\beta_0 & \mathbf{0} & \mathbf{0} \\ \mathbf{0} & \mathbf{F}_{2F} & \mathbf{F}_{2B} & \mathbf{0} & \mathbf{0} & \mathbf{F}_3 \end{bmatrix} \\
\mathbf{Q}_3 &= \begin{bmatrix} \mathbf{0} & \bar{\mathbf{B}}^T_{Fr} & \bar{\mathbf{B}}^T_{Br} & \mathbf{0} & \mathbf{0} & \mathbf{0} \end{bmatrix}^T
\end{aligned} \tag{30}$$

The control output is simply defined as the strain vector of the aircraft. Therefore the output equation is written as

$$\mathbf{y} = \mathbf{C}\mathbf{x} + \mathbf{D}\mathbf{u}_r \tag{31}$$

where

$$\begin{aligned}\mathbf{C} &= \begin{bmatrix} \mathbf{I} & \mathbf{0} & \mathbf{0} & \mathbf{0} & \mathbf{0} & \mathbf{0} \end{bmatrix} \\ \mathbf{D} &= \mathbf{0}\end{aligned} \tag{32}$$

In a special interest, one may want to explore the shaping control development under the varying flight speed (for minimum drag). For a more complex flight controller scheduling, it is desired to understand the wing shaping control algorithm with multiple objectives (minimum drag and alleviated gust load). A common fact to these problems is that the control system matrices are dependent on a linearly varying parameter (flight speed U_∞ or tuning parameter ξ). By taking advantage of this fact, a linear parameter-varying (LPV) approach[21,22] will be used to design the controllers for the wing shaping control under different flight conditions. More details about the controller design will be presented in the final paper.

III. Sample Numerical Results

As the preliminary study, the optimum wing shape of a highly flexible aircraft has been studied for two scenarios. The first considers the optimum wing shapes under varying flight speeds, while in the second case, the wing shape is optimized with the targets of both minimum drag and minimum gust load. However, the shaping controllers are yet to be designed, which will be presented in the final paper.

A. Level Flight Velocity Range: 18 - 28 m/s

An aircraft may experience a wide variety of flight conditions over the course of their flight plane. This will require separate optimum shapes for each different flight condition experienced. This section explores the various optimum wing geometries associated with varying flight velocities that the aircraft might encounter. Specifically, the range of 18 to 28 m/s is explored. Each of these cases is treated as an individual steady level flight case, meaning again only the symmetric modes are considered as design variables. The aircraft model is again trimmed using the traditional control surfaces for each flight velocity in order to have a point of comparison with the optimum solution as well as an initial set of design variables. Some of the trim results are expressed in Table 1 for both the initial and optimum cases. One measure in the effectiveness of the optimization is to examine the percent difference in the thrust required. This gives an idea into the potential energy savings of the optimum wing shape versus the initial wing shape. For this velocity range the varying percent difference is as great as 12.68% and as low as 4.64% meaning the drag reduction is somewhat dependent on the specific flight condition. Figs. 4 to 7 highlight four distinct shapes seen over the velocity range.

Table 1: Initial and optimum trim data for U = 18 to 28 m/s

	Initial			Optimum		
U, m/s	Drag, N	Thrust, N	BAOA, deg	Drag, N	Thrust, N	BAOA, deg
18	105.254	105.974	6.595	100.799	101.061	4.1077
19	95.571	96.011	5.485	90.278	90.468	3.721
20	87.195	87.468	4.528	82.724	82.864	3.353
21	79.943	80.110	3.699	77.479	73.586	3.210
22	73.657	73.756	2.973	66.992	67.085	3.041
23	68.190	68.245	2.333	61.091	61.177	2.940
24	63.424	63.454	1.766	56.053	56.121	2.906
25	59.268	59.282	1.260	51.696	51.763	2.886
26	55.659	55.665	0.803	50.246	50.325	3.140
27	52.520	52.521	0.389	49.733	49.806	3.078
28	49.811	49.811	0.010	41.287	45.604	2.463

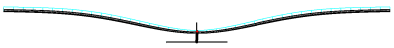

Figure 4: U = 18 m/s

Figure 5: U = 25 m/s

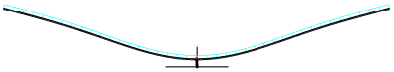

Figure 6: U = 26 m/s

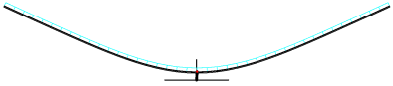

Figure 7: U = 28 m/s

B. Multi Objective Optimization

Using the updated multi-objective function in Eq. (19), a new optimization is performed to study the effects of varying the parameter ξ. For this study, the aircraft is again at 20,000 m and flying at 25 m/s. Only the symmetric modes are used in the optimization as it is still steady level flight. The parameter ξ is varied from 0 to 1 in increments of 0.1. If ξ=1 the optimization is solely to minimize the drag, and if $\xi = 0$ the optimization is solely to minimize the wing root bending moment due to gust disturbances. The results of this study are shown in Table 2 including the aerodynamic drag, thrust, body angle of attack for trim, and the root bending load for each case. It can be seen that as ξ goes from 0 to 1, the drag from the final solution decreases, until it reaches the same solution that was achieved in the single objective function optimization. The bending moment at the root of the wing follows an opposite pattern, increasing as ξ increases. The optimum shapes associated with a few highlighted cases are presented in Figs. 8 to 11. The chosen velocities represent the major shapes seen as ξ is varied.

IV. Final Paper

The final paper will include the highlighted studies above as well as some additional studies. One additional study is to explore the reduced control scheme in order to minimize the control effort required for a given optimization. Another study is to fully develop a linear parameter-varying flight controller to provide the optimum shapes for any flight condition with the guaranteed control performance and stability. This will be applied to both level flight with a varying flight speed as well as level flight transitioning into turning flight. In addition, gust load alleviation and control efforts will be considered in the optimization process to find the best wing shape.

Table 2: Parametric Study Results

ξ	Drag(N)	Thrust(N)	Body AOA(deg)	M_y(N-m)
0	-81.88	82.09	4.16	1.9741×10^3
0.1	-82.19	82.35	3.59	1.9353×10^3
0.2	-81.9	82.15	4.56	1.9916×10^3
0.3	-70.63	70.79	3.95	2.2221×10^3
0.4	-63.93	64.09	4.09	2.4949×10^3
0.5	-58.63	58.74	3.68	2.6965×10^3
0.6	-56.49	56.61	3.49	2.8343×10^3
0.7	-56.39	56.49	3.47	2.8492×10^3
0.8	-54.11	54.19	3.23	3.0317×10^3
0.9	-53.39	53.46	3.10	3.161×10^3
1	-51.66	51.72	2.87	3.1436×10^3

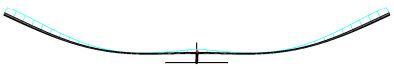

Figure 8: ξ=0

Figure 9: ξ=0.4

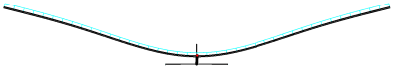

Figure 10: ξ=0.8

Figure 11: ξ=1

Acknowledgments

The research is supported by the Convergent Aeronautics Solutions (CAS) project of NASA ARMD. The views expressed in this paper are those of the authors and do not reflect the official policy or position of NASA or the U.S. Government.

References

[1]Chen, S., Lyu, Z., Kenway, G. K. W., and Martins, J. R. R. A., "Aerodynamic Shape Optimization of Common Research Model WingBodyTail Configuration," *Journal of Aircraft*, Vol. 53, No. 1, 2016, pp. 276–293.

[2]Lyu, Z. and Martins, J. R. R. A., "Aerodynamic Shape Optimization of an Adaptive Morphing Trailing-

Edge Wing," *Journal of Aircraft*, Vol. 52, No. 6, 2015, pp. 1951–1970.

[3]Ghaffarian, S., Field, M., Reynolds, K., Ames, N., Corp, T., Urnes, J., and Louis, S., "Elastically Shaped Wing Optimization and Aircraft Concept for Improved Cruise Efficiency," 2013, pp. 1–44.

[4]Nguyen, N., Kaul, U., Lebofsky, S., Ting, E., Chaparro, D., and Urnes, J., "Development of Variable Camber Continuous Trailing Edge Flap for Performance Adaptive Aeroelastic Wing," 2010.

[5]Nguyen, N. and Ting, E., "Flutter analysis of mission-adaptive wing with Variable Camber Continuous Trailing Edge Flap," *55th AIAA/ASMe/ASCE/AHS/SC Structures, Structural Dynamics, and Materials Conference*, 2014, pp. 1–39.

[6]Sr., J. U., Nguyen, N., Ippolito, C., Totah, J., Trinh, K., and Ting, E., "A Mission-Adaptive Variable Camber Flap Control System to Optimize High Lift and Cruise Lift-to-Drag Ratios of Future N + 3 Transport Aircraft," *51st AIAA Aerospace Sciences Meeting including the New Horizons Forum and Aerospace Exposition, 7-10 January, Grapevine*, 2013, pp. 1–24.

[7]Kota, S., Osborn, R., Ervin, G., Maric, D., Flick, P., and Paul, D., "Mission Adaptive Compliant Wing Design , Fabrication and Flight Test Mission Adaptive Compliant Wing," *Rtompavt*, 2006, pp. 1–19.

[8]Hetrick, J. A., Osborn, R. F., Kota, S., Flick, P. M., and Paul, D. B., "Flight Testing of Mission Adaptive Compliant Wing," *48th AIAAASMEASCEAHSASC Structures Structural Dynamics and Materials SDM Conference*, 2007, pp. 1–17.

[9]Cramer, N. B., Cheung, K., and Swei, S. S.-M., "Design and Testing of a Lattice-based Cellular Component Active Twist Wing," *24th AIAA/AHS Adaptive Structures Conference*, 2016, pp. 1–11.

[10]Jenett, B., Calisch, S., Cellucci, D., Cramer, N., Gershenfeld, N., Swei, S., and Cheung, K. C., "Digital Morphing Wing: Active Wing Shaping Concept Using Composite Lattice-Based Cellular Structures," *Soft Robotics*, Vol. 4, No. 1, 2016, pp. soro.2016.0032.

[11]Su, W., Swei, S. S.-M., and Zhu, G. G., "Optimum Wing Shape of Highly Flexible Morphing Aircraft for Improved Flight Performance," *Journal of Aircraft*, Vol. 53, No. 5, 2017/01/20 2016, pp. 1305–1316.

[12]Su, W. and Cesnik, C. E. S., "Nonlinear Aeroelasticity of a Very Flexible Blended-Wing-Body Aircraft," *Journal of Aircraft*, Vol. 47, No. 5, Sep–Oct 2010, pp. 1539–1553.

[13]Su, W. and Cesnik, C. E. S., "Dynamic Response of Highly Flexible Flying Wings," *AIAA Journal*, Vol. 49, No. 2, Feb 2011, pp. 324–339.

[14]Su, W. and Cesnik, C. E. S., "Strain-Based Analysis for Geometrically Nonlinear Beams: A Modal Approach," *Journal of Aircraft*, Vol. 51, No. 3, MAY-JUN 2014, pp. 890–903.

[15]Su, W. and Cesnik, C. E. S., "Strain-Based Geometrically Nonlinear Beam Formulation for Modeling Very Flexible Aircraft," *International Journal of Solids and Structures*, Vol. 48, No. 16-17, Aug 2011, pp. 2349–2360.

[16]Palacios, R. and Cesnik, C. E. S., "Cross-Sectional Analysis of Nonhomogeneous Anisotropic Active Slender Structures," *AIAA Journal*, Vol. 43, No. 12, Dec 2005, pp. 2624–2638.

[17]Shearer, C. M. and Cesnik, C. E. S., "Nonlinear Flight Dynamics of Very Flexible Aircraft," *Journal of Aircraft*, Vol. 44, No. 5, SEP-OCT 2007, pp. 1528–1545.

[18]Peters, D. A. and Johnson, M. J., "Finite-State Airloads for Deformable Airfoils on Fixed and Rotating Wings," *Proceedings of Symposium on Aeroelasticity anf Fluid Structure Interaction Problems ASME Winter Annual Meeting*, 1994, pp. 1–28.

[19]Tang, D. and Ã, E. H. D., "Experimental and theoretical study of gust response for a wing store model with freeplay," *Journal of Sound and Vibration*, Vol. 295, No. 3, 2006, pp. 659–684.

[20]Aldraihem, O. J., Singh, T., and Wetherhold, R. C., "Optimal Size and Location of Piezoelectric Actuator/Sensors: Practical Considerations," *Journal of Guidance, Control, and Dynamics*, Vol. 23, No. 3, May–Jun 2000, pp. 509–515.

[21]White, A., Zhu, G., and Choi, J., "Optimal LPV Control with Hard Constraints," *International Journal of Control Automation and Systems*, Vol. 14, No. 1, Feb 2016, pp. 148–162.

[22]Zhang, S., Yang, J. J., and Zhu, G. G., "LPV Modeling and Mixed Constrained H-2/H-infinity Control of an Electronic Throttle," *IEEE-ASME Transactions on Mechatronics*, Vol. 20, No. 5, Oct 2015, pp. 2120–2132.